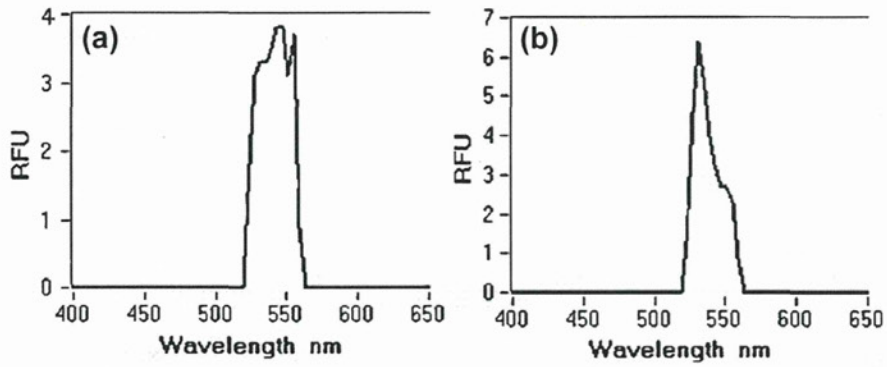

Fig. 1 – (a) SPR observed in Au-OS-MWCNT; (b) SPR observed in Au NP solution.

of optical absorption spectra suggested that there is no adverse influence on the nanoparticles. We noted that Au NPs do not attach to pristine MWCNT (control) when observed after same amount of washing as stated above. Likewise, TEM, EDX and XPS analysis also confirmed the same that no Au NP attachment was done over the pristine MWCNTs under the same set reaction conditions (data not shown).

TEM images of Au-OS-MWCNTs showed gold nanoparticles on the surface of organosulfur modified MWCNTs, as is evidenced in Fig. 2.

Fig. 2b shows TEM micrograph of OS-MWCNT decorated with gold nanoparticles of size 5–15 nm. A micrograph of pristine MWCNT (control) is shown in Fig. 2a for comparison. Gold nanoparticles (without being deposited onto the modified nanotube surface) exhibited face-centered cubic (fcc) structure as indicated by {111} and {200} facet diffraction pattern in Fig. 2d. Fig. 2c shows adherence of several Au NPs along the sidewall of OS-MWCNT. Au NPs attached on the OS-MWCNT surface showed similar fcc-type diffraction pattern associated with Au NPs alone along with the interlayer

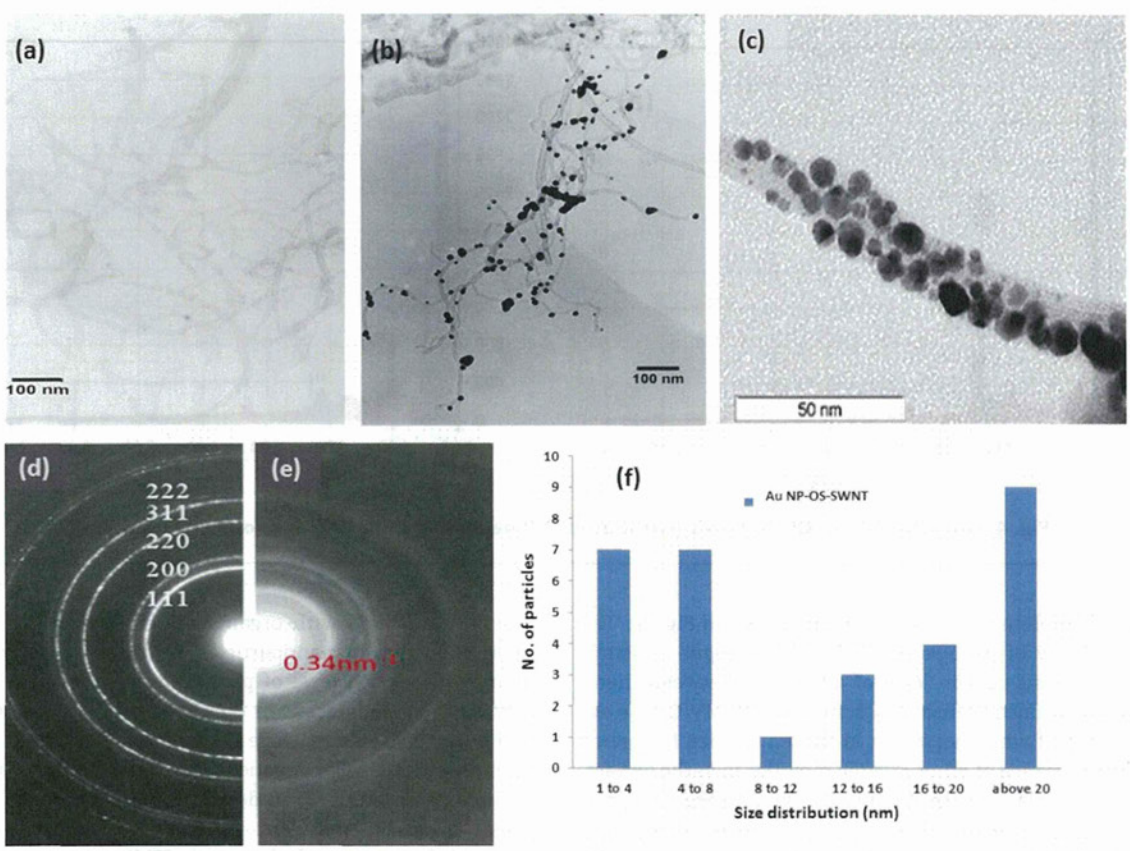

Fig. 2 – (a) TEM image of unmodified CNT; (b) TEM image of Au-OS-MWCNT; (c) High resolution image of Au-OS-MWCNT; (d) XRD pattern obtained from Au NP; (e) XRD pattern obtained from Au-OS-MWCNT; (f) Au NP particle size distribution on OS-MWCNT surface.

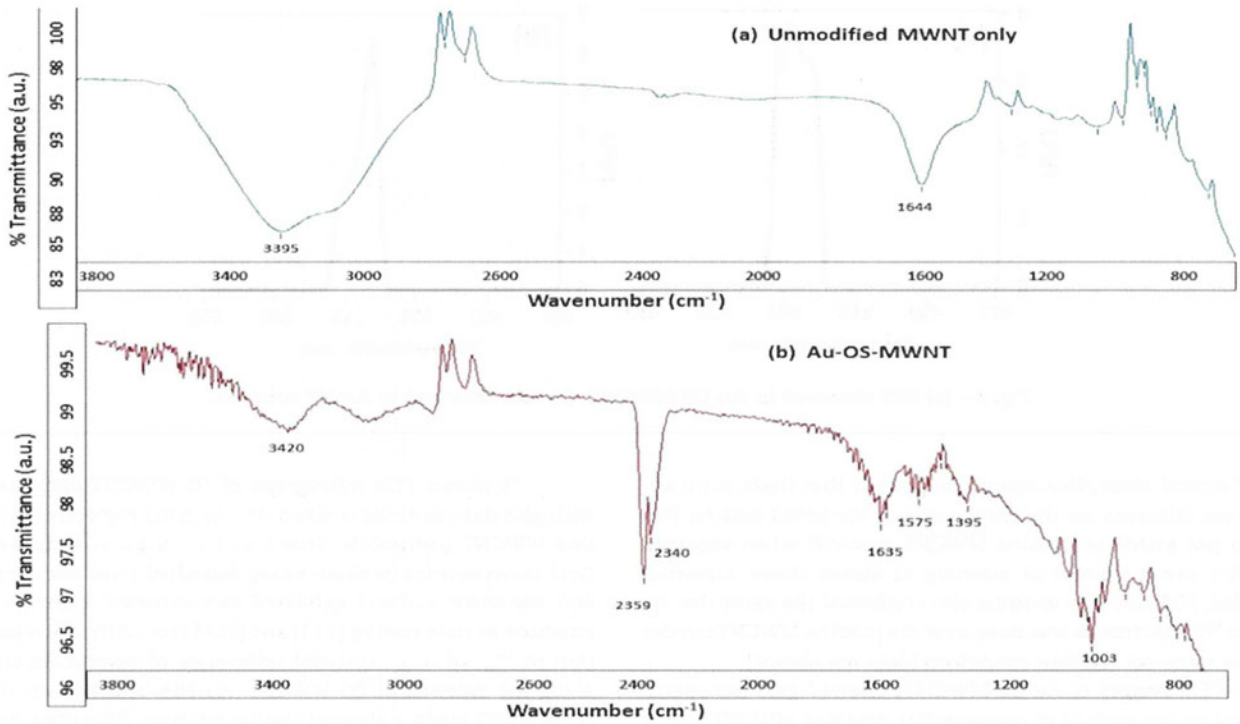

Fig. 3 – (a) FT-IR spectra of unmodified MWCNT; (b) FT-IR spectra of Au-OS-MWCNT.

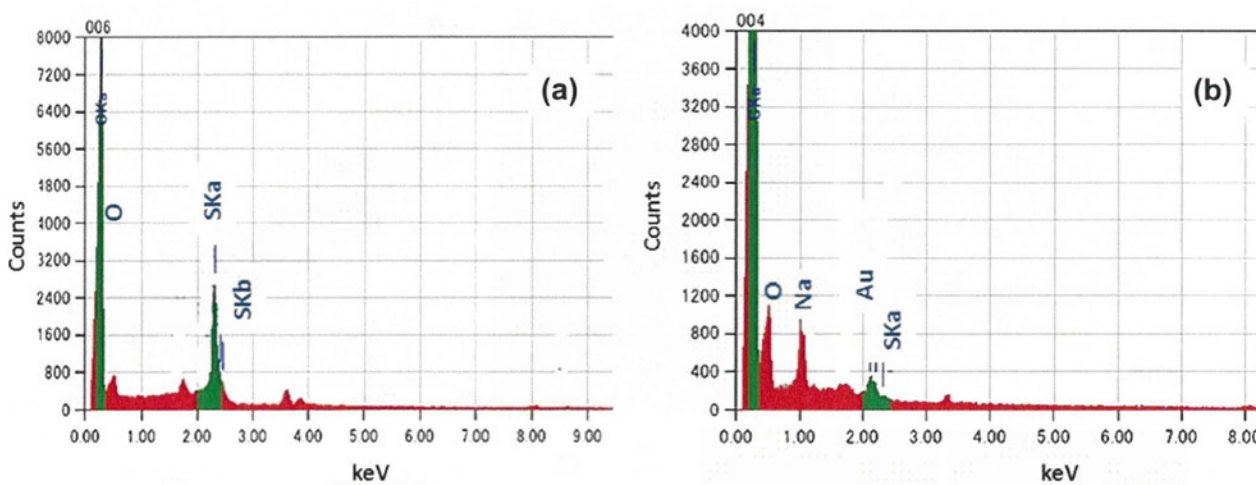

Fig. 4 – (a) EDX data of OS-MWCNT (without Au NP deposition); (b) EDX data of Au-OS-MWCNT.

spacing of graphite sheets (0.34 nm) as shown in Fig. 2e. The close proximity of Au NPs to OS-MWCNT despite constant washing suggests certain level of adherence between them. Average Au NP particle size distribution on OS-MWCNT is depicted in Fig. 2f where variation in the Au NP size happened due to the presence of other organic moieties in garlic extract. This is in accordance with Zhong's [25] finding that the position of nano-gold surface plasmon band depends on particles size, distance between the Au NPs and interaction of Au NPs with molecules on the surface. Red shift (SPR @ 520–540 nm) indicates that either the interparticle spacing is short, or the particle aggregation is bigger. In our cases, if CNTs are successfully modified with organothiol groups on the sidewall of MWCNTs, gold nanoparticles should be closely packed along with certain level of particle aggregation due to other organic moieties present in the garlic extract. This was verified when gold nanoparticle solution was subjected to garlic extract under similar reaction conditions which resulted in particle aggregation. To understand more about active functional groups present over the modified nanotube surface, we carried out transmission mode FT-IR measurements. FT-IR spectrum of unmodified MWCNT is shown in Fig. 3a.

OS-MWCNT decorated with Au NPs (Fig. 3b) showed signature bands at 1635, 1575 and 1395 cm^{-1} associated with the

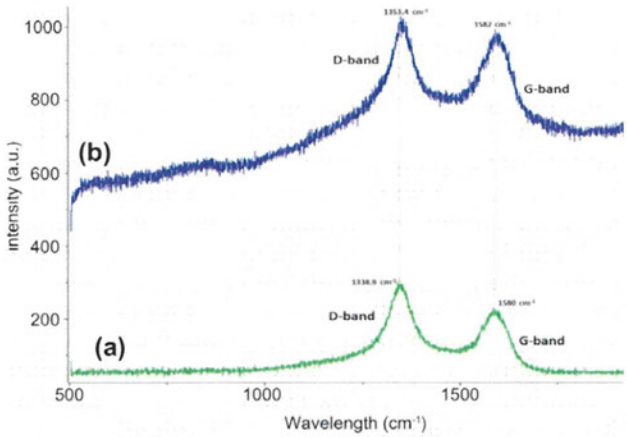

Fig. 5 – Raman spectra of (a) pristine MWCNT and (b) organosulfur modified MWCNT.

stretching of nanotube backbone. Also, evidence of utilizing openings/defects in graphite wall of MWCNT was denoted by characteristic absorbance of —C≡C at 2200–2400 cm^{-1} region. Similar result was obtained by Zhang et al. [26] with nitrile group addition on the sidewall of CNT. It is important to note that the band obtained at 1003 cm^{-1} confirms the presence of thiocarbonyl center whose presence was detected by absorption in 1250–1000 cm^{-1} region. Since, absorption occurs in the same region as C—O stretching, considerable interactions can occur within these vibrations within a single molecule. EDX study (Fig. 4) further confirmed the presence of sulfur in functionalized MWCNT.

Fig. 4a shows EDX spectra of OS-MWCNT (without Au NP attachment) and Fig. 4b shows Au-OS-MWCNT. Gold loading of around 0.78 atomic wt.% was obtained in Au-OS-MWCNT while no such result was obtained from control sample. We also observed the characteristic 2:1 stoichiometric ratio between sulfur and gold at some reaction sites over the Au-OS-MWCNT suggesting formation of dithiols as active biolinker. However, this ratio varied from reaction site being observed over the Au-OS-MWCNT surface. We found that OS-MWCNT can have sulfur content in the range of 0.4–1 atomic wt.%. Upon pyrolysis, the garlic extract confirmed the presence of around 0.17% of sulfur left in the reaction mixture. Further, the initial sulfur concentration in the organosulfur extract was found to be around 1.8%.

Surface modification was confirmed by Raman spectroscopy as shown in Fig. 5.

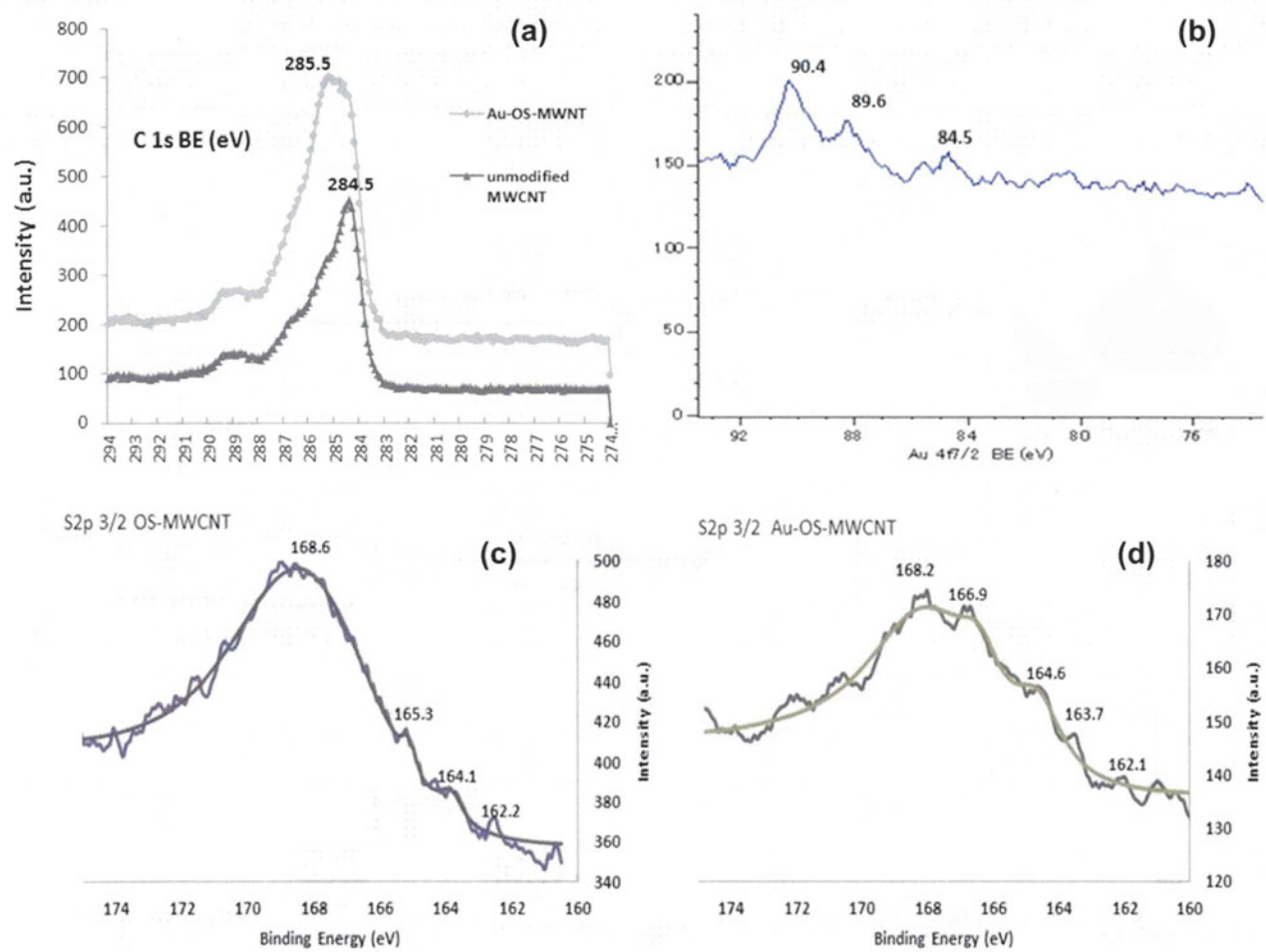

Fig. 6 – XPS spectra (a) C 1s spectra of modified and unmodified MWCNTs; (b) Au 4f spectra of Au NPs attached onto Au-OS-MWCNTs; (c) S 2p spectra of OS-MWCNT; (d) S 2p spectra of Au-OS-MWCNTs.

Fig. 5a shows Raman spectra of pristine MWCNTs while Fig. 5b shows that of OS-MWCNTs. Pristine MWCNTs showed G and D bands at 1580 and 1338.9 cm^{-1}, respectively. These G and D bands got shifted to 1582 and 1353.4 cm^{-1}, respectively in case of OS-MWCNTs. The higher upshift in D-band region towards the higher wavelength and lower shift in G-band is commonly observed in case of dopants containing oxygen atoms in their structure. It is known that oxygen can easily get attached to the defect sites in nanotube network leading to greater modification in defect band [27]. Further, the G/D intensity ratio of pristine MWCNTs (1.18) as compared to OS-MWCNTs (1.16) suggests decrease in relative sample purity due to CNT surface modification. These chemical modification results in the upshift of G and D bands which are related to direct electron charge transfer process from the nanotube to the acceptor molecule and are generally time-dependent [28]. Thus, Raman spectra confirmed the surface modification took place while FT-IR and EDX suggested towards the presence of sulfur (organothiols) in the reaction mixture. Confirmatory proof of organosulfur modified nanotube surface with facilitating Au NP attachment was obtained by XPS data as shown in Fig. 6.

In present case (Fig 6a), unmodified MWCNT C1 component of C 1s spectrum was represented at 284.5 eV [29]. This when compared to Au-OS-MWCNT composite showed an increase of C 1s spectral peak width upon functionalization, from 1.4 to 1.9 eV. This is expected when electron delocalization becomes limited [30,31] as a result of interactions between thiols and CNT sidewall. Broadening is also observed due to overlapping of CNT and organosulfur C 1s spectral envelopes, which causes an increased intensity in binding energy region around 286.5 eV [32] (C-SH) as observed in our case. Both contributions are manifested as increases in peak width and asymmetry. OS-MWCNTs after treatment with Au NP solution exhibits a new peak at Au 4f region (Fig. 6b) together with C 1s peak at 285.5 eV and S 2p peak between the regions 162–164 eV responsible for thiol interactions. In Fig. 6b, component at 84.5 eV (88.2 for the 4f5/2 component) is assigned to Au^0. In particular, the positions of the Au 4f7/2 signal assigned to the Au^0 peak present a binding energy sensitively higher respect to the 84 eV value of bulk gold (88 eV for the 4f5/2 component). This is an indication of the presence of very small gold nanoclusters in the samples due to the presence of metallic nuclei that acts as centers for the successive grow of the gold nanoparticles. This can also result from the coalescence of Au NPs when deposited over the OS-MWCNTs as observed in this study. Further, decrease in relative peak intensities between the two S 2p spectra (Fig. 6c and d) can be clearly observed after Au NP attachment which further supports that S-moieties are responsible for Au NP attachment. Characteristic sulfur–oxygen interaction at around 168 eV region was also observed which is common in case of natural organosulfurs. This confirms that the attachment of Au-NPs to modified CNT surface can be achieved via thiol and thiocarbonyl linkages. Similar results were reported by Nakamura et al. [33] for carbon surface modification via elemental sulfur and subsequent interaction with Au NPs.

Finally, based upon our experimental observation, we were able to hypothesize a free-radical mechanism (Fig. 7) which may be responsible for CNT surface modification in presence of alliin/allicin as major organosulfur groups in garlic. The

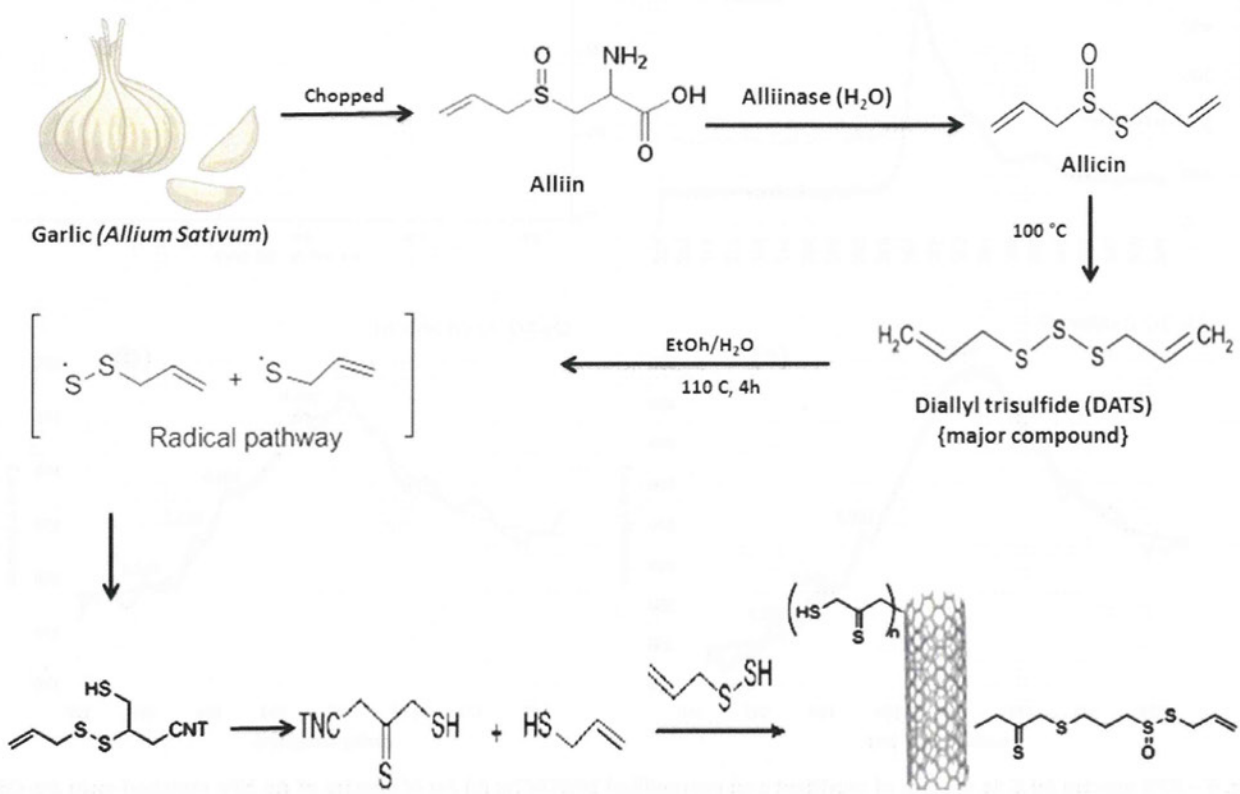

Fig. 7 – Schematic representation of MWCNT surface modification in presence of garlic organosulfur extract.

thiolated CNTs obtained as end-product can then be used for Au NPs deposition over the modified nanotube surface.

These results clearly demonstrate that organosulfur groups (alliin/allicin as major products) present in the garlic extract are responsible for attachment of Au NPs over the modified nanotube surface and in absence of these 'bio-linkers', no Au NP attachment was observed. We strongly believe that biogenic methods have the potential to provide advanced surface/material modification strategies in the growing field of carbonaceous materials.

4. Summary

We have shown 'one-pot' sidewall attachment of Au NPs to MWCNTs treated with garlic plant extract (organosulfurs) by a facile eco-friendly process. As per our knowledge, this is the first study to effectively utilize plant phytochemicals for sidewall modification of CNTs under moderate temperature conditions. Such bio-inspired materials may facilitate novel synthesis and application routes in a more sustainable manner. Finally, an interdisciplinary research will aid in better understanding of underlying mechanism and properties this nanocomposite may possess.

Acknowledgements

This work was partly supported by Special Coordination Fund for Promoting Science and Technology, Creation of Innovative Centers for Advanced Interdisciplinary Research Areas (Innovative Bioproduction Kobe) from the Ministry of Education, Culture, Sports and Technology (MEXT) and partly by the MEXT Scholarship research fund.

We would like to make a noteworthy mention along with sincere thanks to Dr. Yuzuru Mizuhata who provided us with extensive technical support necessary for the completion of this research. Also, we would like to thank the members of his research group including Takashi Hasegawa, Kaori Takeda and Akihito Katayama for assisting us in our research. Also, we would we extend our sincere gratitude to Dr. Yasukiyo Ueda for his assistance with TEM observations. We also thank Dr. Vasudevan Dhayalan (LMU, Germany) for his kind assistance in understanding the chemical mechanism proposed in this research.

REFERENCES

[1] Tasis D, Tagmatarchis N, Bianco A, Prato M. Chemistry of carbon nanotubes. Chem Rev 2006;106(3):1105–36.
[2] Dai H. Carbon nanotubes: synthesis, integration, and properties. Acc Chem Res 2002;35(12):1035–44.
[3] El-Sayed MA, Eustis S. Why gold nanoparticles are more precious than pretty gold: noble metal surface plasmon resonance and its enhancement of the radiative and nonradiative properties of nanocrystals of different shapes. Chem Soc Rev 2006;35(3):209–17.
[4] Satishkumar BC, Vogl EM, Govindaraj A, Rao CNR. The decoration of carbon nanotubes by metal nanoparticles. J Phys D Appl Phys 1996;29(12):31273–6.
[5] Jiang K, Eitan A, Schadler LS, Ajayan PM, Siegel RW. Selective attachment of gold nanoparticles to nitrogen-doped carbon nanotubes. Nano Lett 2003;3(3):275–7.
[6] Eitan A, Jiang K, Dukes D, Andrews R, Schadler LS. Surface modification of multiwalled carbon nanotubes: toward the tailoring of the interface in polymer composites. Chem Mater 2003;15(16):3198–201.
[7] Parthasarathy R, Lin X, Jaeger HM. Electronic transport in metal nanocrystals arrays: the effect of structural disorder on scaling behavior. Phys Rev Lett 2001;87(18):1868071–4.
[8] Ellis AV, Vijayamohan K, Goswami R, Chakrapani N, Ramanathan LS, Ajayan PM, et al. Hydrophobic anchoring of monolayer protected gold nanoclusters to carbon nanotubes. Nano lett 2003;3(3):279–82.
[9] Zhang R, Hummelgard M, Olin H. Simple and efficient gold nanoparticles deposition on carbon nanotubes with controllable particle sizes. Mater Sci Eng B 2009;158:48–52.
[10] Shia Y, Yangb R, Yueta PK. Easy decoration of carbon nanotubes with well dispersed gold nanoparticles and the use of the material as an electrocatalyst. Carbon 2009;47:1146–51.
[11] Gingery D, Bühlmann P. Formation of gold nanoparticles on multiwalled carbon nanotubes by thermal evaporation. Carbon 2009;46:1966–72.
[12] Hu H, Bhowmik P, Zhao B, Hamon MA, Itkis ME, Haddon RC. Determination of the acidic sites of purified single walled carbon nanotubes by acid–base titration. Chem Phys Lett 2001;345(1):25–8.
[13] Zhao J, Park H, Han J, Lu JP. Electronic properties of carbon nanotubes with covalent sidewall functionalization. J Phys Chem B 2004;108(14):4227–30.
[14] Zanella R, Basiuk EV, Santiago P, Basiuk VA, Mireles E, Puente-Lee I, et al. Deposition of gold nanoparticles onto thiol-functionalized multiwalled carbon nanotubes. J Phys Chem B 2005;109(34):16290–5.
[15] Banerjee S, Wong SS. Synthesis and characterization of a novel nanotube–nanocrystal heterostructure. Nano Lett 2002;2(3):195–200.
[16] Zhao L, Gao L. Coating multi-walled carbon nanotubes with zinc sulphide. J Mater Chem 2004;14(6):1001–4.
[17] Harpovic S, Liu Y, Male KB, Luong JHT. Electrochemical biosensing platforms using platinum nanoparticles and carbon nanotubes. Anal Chem 2004;76(4):1083–8.
[18] Amagase H, Petesch BL, Matsuura H, Kasuga S, Itakura Y. Intake of garlic and its bioactive components. J Nutr 2001;131(3). 955S–62S.
[19] Volk GM, Stern D. Phenotypic characteristics of ten garlic cultivars grown at different north american locations. Hortscience 2009;44(5):12238–47.
[20] Lawson LD, Hughes BD. Characterization of the formation of allicin and other thiosulfinates from garlic. Planta Med 1992;58(4):345–50.
[21] Kamel A, Saleh M. Recent Studies on the Chemistry and Biological Activities of the Organosulfur Compounds of Garlic (*Allium sativum*) Studies in Natural Products Chemistry. Amsterdam: Elsevier; 2000.
[22] Bahr JL, Tour JM. Covalent chemistry of single-wall carbon nanotubes. J Mater Chem 2002;12(7):1952–8.
[23] Basiuk VA, Kobayashi K, Kaneko T, Negishi Y, Basiuk EV, Saniger-Blesa JM. Irradiation of single-walled carbon nanotubes with high energy protons. Nano Lett 2002;2(7):789–91.
[24] Kimling J, Maier M, Okenve B, Kotaidis V, Ballot H, Plech A. Turkevich method for gold nanoparticle synthesis revisited. J Phys Chem B 2006;110(32):15700–7.
[25] Zhong Z, Patskovskyy S, Bouvrette P, Luong JHT, Gedanken A. The surface chemistry of Au colloids and their interactions

with functional amino acids. J Phys Chem B 2004;108(13):4046–52.
[26] Zhang M, Su L, Mao L. Surfactant functionalization of carbon nanotubes (CNTs) for layer-by-layer assembling of CNT multi-layer films and fabrication of gold nanoparticle/CNT nanohybrid. Carbon 2006;44(2):276–83.
[27] Graupner R, Abraham J, Vencelova A, Seyller T, Hennrich F, Kappes MM, et al. Doping of single-walled carbon nanotube bundles by BrØnsted acids. Phys Chem Chem Phys 2003;5(24):5472–6.
[28] Souza Filho AG, Meunier V, Terrones M, Sumpter BG, Barros EB, Villalpando-Paez F, et al. Selective tuning of the electronic properties of coaxial nanocables through exohedral doping. Nano Lett 2007;7(8):2383–8.
[29] Xing Y, Li L, Chusuei CC, Hull RV. Sonochemical oxidation of multiwalled carbon nanotubes. Langmuir 2005;21(9):4185–90.
[30] Yang D-Q, Sacher E. Carbon 1s X-ray photoemission line shape analysis of highly oriented pyrolytic graphite: the influence of structural damage on peak asymmetry. Langmuir 2006;22(3):860–2.
[31] Yang D-Q, Sacher E. S-P hybridization in highly oriented pyrolytic graphite and its change on surface modification, as studied by X-ray photoelectron and Raman spectroscopies. Surf Sci 2002;504:125–37.
[32] Yang D-Q, Hennequin B, Sacher E. XPS demonstration of pi–pi interaction between benzyl mercaptan and multiwalled carbon nanotubes and their use in the adhesion of Pt nanoparticles. Chem Mater 2006;18(21):5033–8.
[33] Nakamura T, Ohana T, Hagiwara Y, Tsubota T. Photochemical modification of diamond powders with elemental sulfur and their surface-attachment behavior on gold surfaces. Phys Chem Chem Phys 2009;11(4):730–4.

Srivastava et al. Nanoscale Research Letters 2013, 8:70
http://www.nanoscalereslett.com/content/8/1/70

Nanoscale Research Letters
a SpringerOpen Journal

NANO EXPRESS Open Access

Biogenic synthesis and characterization of gold nanoparticles by *Escherichia coli* K12 and its heterogeneous catalysis in degradation of 4-nitrophenol

Sarvesh Kumar Srivastava[1], Ryosuke Yamada[2], Chiaki Ogino[1] and Akihiko Kondo[1*]

Abstract

Room-temperature extracellular biosynthesis of gold nanoparticles (Au NPs) was achieved using *Escherichia coli* K12 cells without the addition of growth media, pH adjustments or inclusion of electron donors/stabilizing agents. The resulting nanoparticles were analysed by ultraviolet–visible (UV–vis) spectrophotometry, atomic force microscopy, transmission electron microscopy and X-ray diffraction. Highly dispersed gold nanoplates were achieved in the order of around 50 nm. Further, the underlying mechanism was found to be controlled by certain extracellular membrane-bound proteins, which was confirmed by Fourier transformation-infrared spectroscopy and sodium dodecyl sulfate polyacrylamide gel electrophoresis. We observed that certain membrane-bound peptides are responsible for reduction and subsequent stabilization of Au NPs (confirmed by zeta potential analysis). Upon deactivation of these proteins, no nanoparticle formation was observed. Also, we prepared a novel biocatalyst with Au NPs attached to the membrane-bound fraction of *E. coli* K12 cells serving as an efficient heterogeneous catalyst in complete reduction of 4-nitrophenol in the presence of $NaBH_4$ which was studied with UV–vis spectroscopy. This is the first report on bacterial membrane-Au NP nanobiocomposite serving as an efficient heterogeneous catalyst in complete reduction of nitroaromatic pollutant in water.

Keywords: Gold nanoparticles, Extracellular biosynthesis, Green catalysis, *Escherichia coli*, Nitrophenol degradation, Water treatment

Background

Gold nanoparticle (Au NP), being the most stable mono-metallic nanoparticle, promises to be a key material and building block for newer technologies in the twenty-first century. Gold in its bulk state is regarded as a noble metal and is very unreactive because of its completely filled d-band [1]. However, at nanoscale, it is proving to be an important material for catalysis owing to its shape, size and crystal structure arrangement [2]. Due to this new set of properties, it has found wide-scale application in optics, electronics, catalysis, fabrication and biomedical utilities [3]. Generally speaking, physical methods of producing gold nanoparticles involve heating of gold at reduced pressure to generate gold vapour, while chemical synthesis requires a reducing agent (generally citrate) followed by addition of a stabilizing agent [4-7]. However, these chemical methods deliver at the cost of expensive reducing and capping agents and toxic solvents along with tedious process control. To overcome these issues, several biogenic synthesis processes have been reported owing to the constant need for cost-effective eco-friendly synthesis of Au NPs. Microbial systems have found an important role in nanoparticle production due to their natural mechanism for detoxification of metallic ions through reduction which can be achieved extracellularly or intracellularly through bioaccumulation, precipitation, biomineralization and biosorption. Ogi et al. [8] showed gold nanoparticle formation in the presence of H_2 gas pumped with *Shewanella algae* cell extract.

* Correspondence: akondo@kobe-u.ac.jp
[1]Department of Chemical Science and Engineering, Graduate School of Engineering, Kobe University, 1-1 Rokkodai-cho, Nada, Kobe 657-8501, Japan
Full list of author information is available at the end of the article

Similarly, gold nanoparticles of different shapes and sizes were produced using bacterial and fungal strains [9-12]. However, apart from the stated advantages, biological synthesis suffers from poor mono-dispersity, random aggregation, non-uniform shapes, problems in scale-up, etc. [13]. Though, in recent times, many organisms have been reported to produce nanoparticles, scientific understanding on the mechanism and the machinery related to its production is still in its infancy. Therefore, there is a need to improve upon this green synthesis process with an aim to understand the underlying mechanism and design a working prototype for biomimetic production of Au NPs.

These nanoparticles, upon being adhered to a matrix, may serve as a better catalyst than bulk metal due to greater accessibility to surface atoms and low coordination number especially in the case of water treatment. Among several water pollutants, nitroaromatic compounds are considered as the most toxic and refractory pollutants, of which the permissible range is as low as 1 to 20 ppb. However, these are common in production of dyes, explosives and pesticides among many others; thus, their industrial production is considered as an environmental hazard [14]. Upon being released into the environment, these nitrophenols pose significant public health issues by exhibiting carcinogenic and mutagenic potential in humans [15].

Normally, it takes a long time for degradation of nitrophenols in water which poses considerable risk if it seeps into aquifers along with the groundwater. These nitrophenols tend to get accumulated in deep soil and stays indefinitely. Although several water treatment methods are available like chemical precipitation, ion exchange adsorption, filtration and membrane systems, they are slow and non-destructive. Therefore, there is a need to remove these highly toxic compounds with efficient catalytic systems. Generally, nanoparticles are immobilized onto supporting materials like silica, zeolites, resins, alumina, microgels, latex, etc. which are inert to the reactants and provide a rigid framework to the nanoparticles. The gold-supported catalysts can then be used to carry out partial or complete oxidation of hydrocarbons, carbon monoxide, nitric oxide, etc. [16]. In a recent study, Deplanche et al. [17] showed coating of palladium followed by gold over *Escherichia coli* surface in the presence of H_2 to produce biomass-supported Au-Pd core-shell-type structures and subsequent oxidation of benzyl alcohol. Likewise, we believe that bacterial biomass is essentially carbonaceous matter which can be used to serve as a matrix for preparing a heterogeneous catalyst with the incorporation of nanoparticles. With this aim, we utilized *E. coli* K12 strain to check its potential for producing Au^0 from $AuCl_4^-$. This strain has been known for its reduction activity as shown with bioremediation studies [18,19]. Here, we report bioreduction of gold cations at room temperature to yield well-dispersed nanoparticles (Au^0). The resulting nanoparticles were characterized by ultraviolet–visible (UV–vis) spectroscopy, atomic force microscopy (AFM), selected-area electron diffraction (SAED), transmission electron microscopy (TEM) and X-ray diffraction (XRD). Additionally, the extracellular reduction mechanism was examined by Fourier transformation-infrared spectroscopy (FT-IR), zeta potential (Z-pot) and sodium dodecyl sulfate polyacrylamide gel electrophoresis (SDS-PAGE). We observed that certain membrane-embedded proteins in the extracellular membrane fraction of the cell are responsible for reducing gold cation to stable Au^0 state. Further, these membrane-bound gold nanoparticles were utilized to produce a heterogeneous catalyst in degradation of 4-nitrophenol (4-NP). This biosynthesis study provides an excellent platform for the production of gold nanoparticles by bacterial membrane-bound proteins. The resulting membrane-bound nanoparticles can be prepared into an eco-friendly cost-effective bionanocomposite to serve as an efficient catalyst in complete degradation of 4-nitrophenol.

Methods

Bacterial strain and growth conditions

E. coli K12 cells were procured from our existing strain collection and were cultured in nutrient broth (10 g L^{-1} peptone, 10 g L^{-1} meat extract, 0.5 g L^{-1} NaCl) at 27°C and 120 rpm for 24 h in screw-capped flasks. After a day of incubation, the culture was centrifuged at 10,000×*g* for 10 min, and the resulting bacterial pellet was separated and retained. The bacterial pellet was thoroughly washed three times in sodium saline followed by washing three times in Milli-Q water (Millipore, Tokyo, Japan) to remove any unwanted material sticking to the cells. These cells were weighed, and 0.5 g wet weight of pellet was prepared to be used later. The washed cells suspended in 10 mL of distilled water gave a solution with a cell concentration of 5.2×10^{11} cells mL^{-1}.

To determine whether or not intact cells were required for Au NP formation, *E. coli* K12 cells were cultured and harvested as in the previously described method. The cells were then disrupted by autoclaving (120°C at 15 psi for 30 min). This caused complete lysis of the bacterial cells which were later centrifuged at 15,000×*g* for 60 min to separate the membrane fraction (pellet) from the soluble (supernatant) fraction. Membrane-bound fraction (MBF) pellet was pooled together and washed thrice with Milli-Q water and re-centrifuged again at 15,000×*g* for 30 min. Finally, 2 g of MBF pellet (wet wt.) was retained to be incorporated with 10 mL of 0.01 M $HAuCl_4$ solution (Nacalai Tesque, Kyoto, Japan). Although pH was measured at this stage (pH 2.8), no

adjustment was made. Control reactions included 0.01 M $HAuCl_4$ solution prepared with soluble (supernatant) fraction and uninoculated $HAuCl_4$ solution prepared with Milli-Q water.

Characterization of biogenic gold nanoparticles

UV-visible spectra were obtained using a Hitachi U2000A UV–vis spectrophotometer (Tokyo, Japan). The formation of Au NPs was monitored by UV–vis spectra of the reaction mixture from 210 to 800 nm.

Primary study of nanoparticle shape and size was carried out using an SPI-3800N atomic force microscope with SPA 400 soundproof housing sample holder connected to an imaging system (Seiko Instruments, Chiba, Japan). Five microlitres was taken from the reaction mixture and placed on the glass grid and dried at room temperature. The images were obtained using SPIWin (3800N) ver. 3.02J (Wyandotte, MI, USA).

Morphology and grain size of these nanoparticles were analysed using a Hitachi H-7100 transmission electron microscope. Two microlitres was taken from the two reaction mixtures and placed on carbon-coated copper grids and dried at room temperature. The transmission electron micrographs and the SAED patterns were recorded at an acceleration voltage of 100 kV. The images were analysed using the ImageJ 1.43M software.

FT-IR analysis was done using Jasco FT/IR-680 plus (Easton, MD, USA) coupled to a high-performance computer. The samples (100 μL) were placed over the ATR analyser, and the resulting spectra were analysed using Spectra Manager ver. 1.06.02. Zeta potential measurements were performed using the Malvern Zetasizer Nano ZS model ZEN3600 (Malvern, UK) equipped with a standard 633-nm laser.

Confirmatory study of resulting Au NPs was done by XRD using a Rigaku RINT-TTR diffractometer (Tokyo, Japan) equipped with a parallel incident beam (Göbel mirror) and a vertical θ-θ goniometer. Samples were placed directly on the sample holder. The X-ray diffractometer was operated at 50 kV and 300 mA to generate CuKα radiation. The scan rate was set to 5° mil^{-1}. Identification of the metallic gold was obtained from the JCPDS database.

Preparation of biomass-supported Au nanocatalyst in 4-nitrophenol degradation

The reduction of 4-NP by $NaBH_4$ was studied as a model reaction to probe catalytic efficiency of a biomass-supported Au catalyst for heterogeneous systems. Under experimental conditions, reduction does not proceed at all simply with the addition of $NaBH_4$ or biomass alone. However, in the presence of a biomass-supported Au catalyst, it proceeds to completion with formation of 4-aminophenol (4-AP). To study the reaction in a quartz cuvette, 2.77 mL of water was mixed with 30 μL (10^{-2} M) of 4-NP solution and 200 μL of freshly prepared $NaBH_4$ (10^{-1} M) was added. The Au NP reaction mixture along with the MBF was dried for 24 h at 90°C, and 5 mg of biomass-Au NP composite (size approximately 50 nm, 4.2×10^{-6} mol dm^{-3}) was added to the above reaction mixture. A similar technique was used by Narayanan and Sakthivel [20] by coating fungal mycelia-coated Au NPs on glass beads. UV–vis spectra of the sample were recorded at every 2-min interval in the range of 200 to 600 nm. The rate constant of the reduction process was determined by measuring the change in absorbance of the initially observed peak at 400 nm, for the nitrophelate ion as the function of time.

Results and discussion

Characterization of biogenic Au NPs

Gold nanoparticle formation was primarily observed by UV–vis spectroscopy and AFM. After a series of experimentations, we found that MBF of *E. coli* K12 strain has certain proteins which are responsible for reducing Au cations into Au NPs. A distinct pink colour was observed due to the phenomenon of surface plasmon resonance (SPR) [21] (Figure 1a) in the reaction mixture containing MBF of the bacterial cell after 24 h. No colour formation was present in the control sample consisting of soluble fraction (Figure 1b) and gold ion solution without inoculum (Figure 1c). The same is shown in the inset of Figure 1. UV–vis spectra (Figure 1) of aqueous reaction mixtures showed no increase in absorbance after 24 h, suggesting formation of stable nanoparticles in the reaction mixture. It should be noted that the SPR peak broadening and associated decreased intensity is because of the interaction between the membrane fraction and Au NPs in the reaction mixture. [22] This can be understood by the fact that when these Au NPs are in the vicinity of bacterial cells, membrane fraction or lipopolysaccharides, they tend to adhere to these substrates, thereby reducing the peak intensity (adding scattering background) as compared to otherwise observed SPR of Au NPs alone. This also suggests that in the case of biogenic synthesis of nanoparticles, the presence and intensity of SPR should not be the sole criterion for concentration assessment.

It is important to note that no colour change was observed in control solutions consisting of cell soluble fraction and gold cation solution (without inoculum), suggesting the absence of nanoparticle formation. This was further verified when these samples were examined by AFM as shown in Figure 2.

The AFM probe detected discrete circular nanoparticles (Figure 2a,b) from the MBF reaction mixture, while no such formation was observed in the soluble fraction or gold cation solution without inoculum (Figure 2c,d).

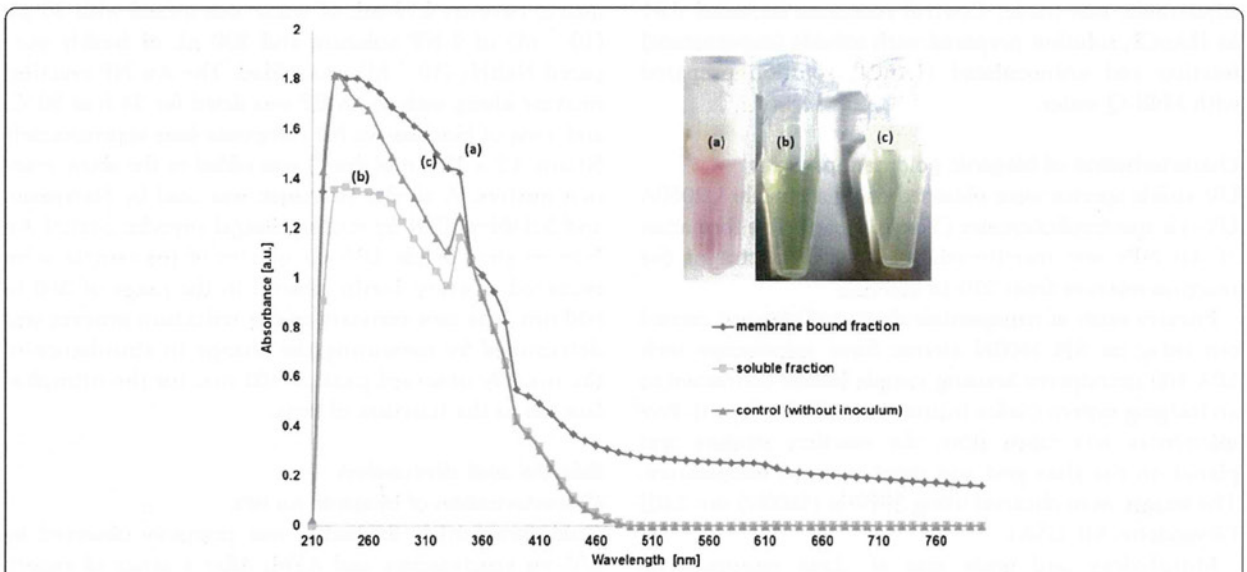

Figure 1 UV–vis spectra observed after 24 h. (**a**) SPR due to Au NP produced by MBF; (**b**) no SPR absorbance in soluble fraction; (**c**) no SPR absorbance in gold ion solution without inoculum. The inset figure corroborating the same in the above-mentioned samples, respectively.

The 2D profile obtained by AFM suggested strong shape control (circular) with a size around 50 nm. This strong shape control indicated that apart from reducing proteins present in the MBF, certain organic groups must be acting as stabilizing agent. To investigate the same, the membrane-bound reaction mixture was subjected to FT-IR analysis to analyse the chemical groups responsible for nanoparticle synthesis. FT-IR spectra (Figure 3a) showed distinct absorption in the region 1,800 to 1,600 cm^{-1} responsible for amide linkages in the reaction mixture.

FT-IR spectra (Figure 3a) confirmed the presence of vibration bands centred at 1,841, 1,787, 1,756, 1,725, 1,692, 1,680, 1,661, 1,650, 1,634 and 1,603 cm^{-1}. This

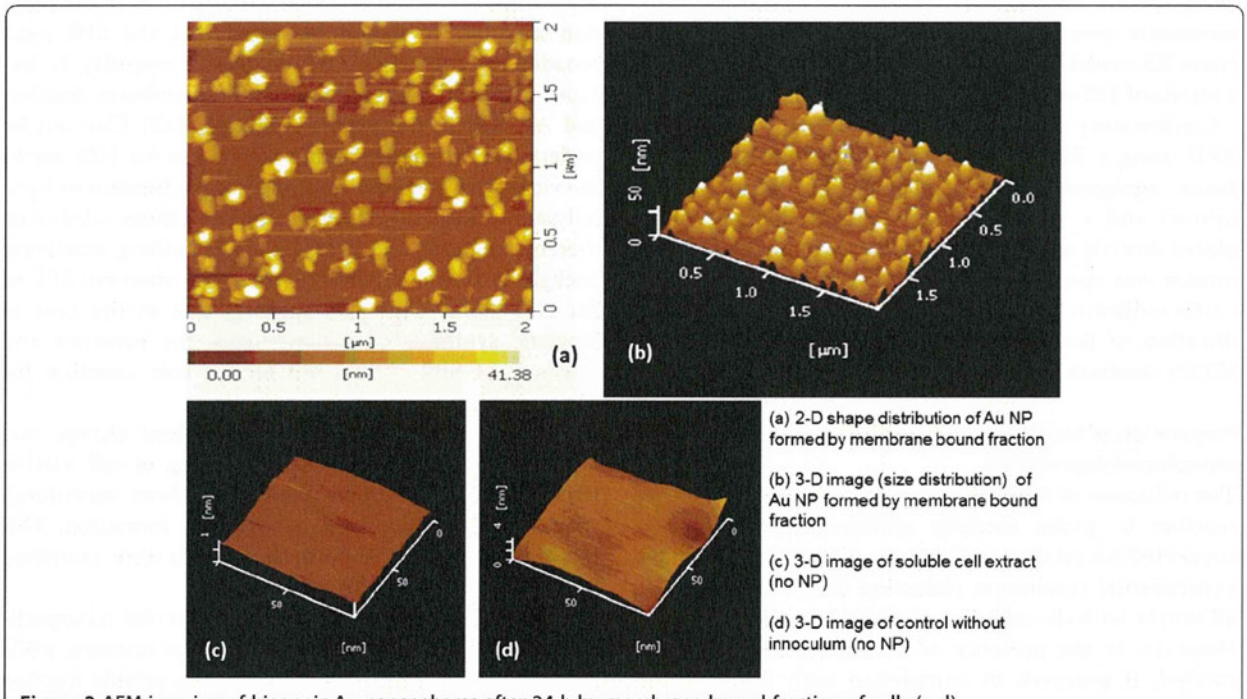

Figure 2 AFM imaging of biogenic Au nanospheres after 24 h by membrane-bound fraction of cells (a-d).

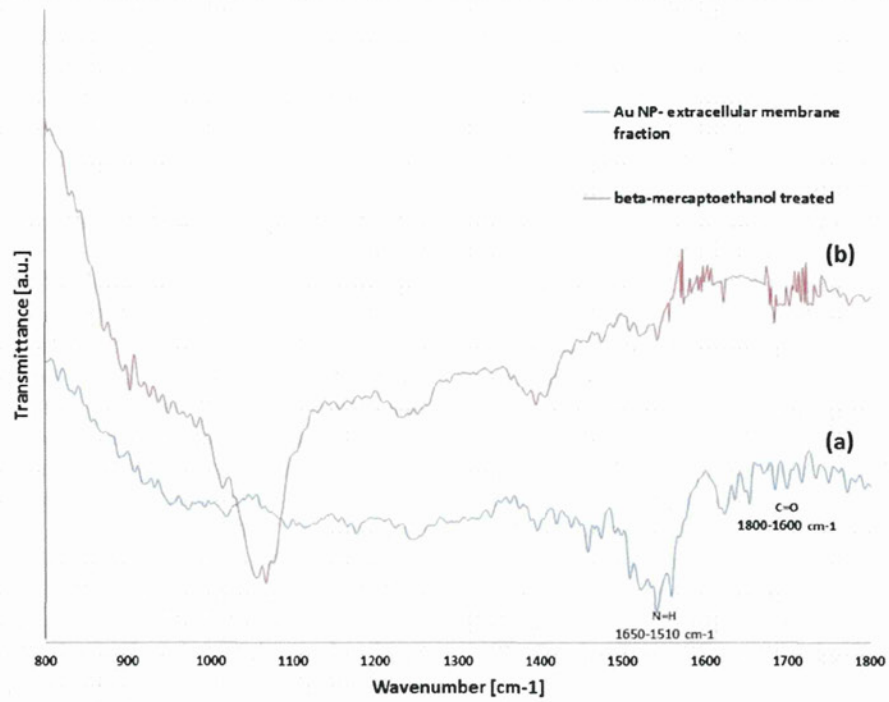

Figure 3 FT-IR spectra of reaction solution. (**a**) Membrane-bound fraction with Au NPs (indicated in blue); (**b**) membrane-bound fraction treated with β-mercaptoethanol (indicated in red).

highlights the presence of amide I (C=O) and amide II (N=H) groups present in the reaction mixture. It is likely that the amide carbonyl group (C=O) arises from peptide coupling in proteins from the extracellular membrane fraction of the bacterial cell. This supports the fact that the secondary amide C=O stretching which forms protein/Au bioconjugates may have a role in stabilization of nanoparticles [23]. Generally, in the case of biogenic synthesis, the presence of active chemical groups like amino, sulfhydryl and carboxylic groups plays a key role in reduction of metallic ions and subsequent formation of nano/microparticles. Since amino and carboxyl groups were detected by FT-IR, it strongly suggested towards the presence of certain proteins in the reaction medium responsible for Au NP biosynthesis. Further, aqueous stability of Au NPs were tested by zeta potential analysis. It should be noted that if active groups on biomass carry greater positive charge at low pH, it weakens the reducing power of biomass and allows $AuCl_4^-$ ions to get closer to the reaction site [24]. This decreases the reaction rate and causes strong biosorption between Au NPs and biomass resulting in particle aggregation. Since the bacterial cell wall of *E. coli* is negatively charged, it tends to thermodynamically favour the formation of nanoparticles at low pH as observed in our case. This was confirmed by zeta potential analysis of the Au NP solution with a mean Z-pot of −24.5 ± 3.1 mV, suggesting a stable gold colloid solution. To further investigate the role of proteins in nanoparticle formation, MBF was treated with 1% β-mercaptoethanol (β-met) and heated for 30 min at 95°C. This treatment caused disruption of disulfide bonds within the multimeric chains of peptide and eventually resulted in loss of activity. In the absence of reducing activity by membrane-bound proteins, no nanoparticle formation was observed with β-met-treated MBF. This was further verified by FT-IR analysis (Figure 3b) with disappearance of most bands around the 1,600 cm^{-1} region. The peak observed at 1,075 cm^{-1} corresponds to the thiocarbonyl group due to the addition of mercaptoethanol in the reaction mixture. This suggested that certain membrane-embedded proteins may be responsible for reducing Au^{3+} to Au nanoparticles (Au^0). The membrane proteins responsible for nanoparticle synthesis were run along with β-met-treated membrane proteins in SDS-PAGE gel (data not shown) which confirmed the presence of different sizes of protein bands in the reaction mixture, of which 25 and 73 KDa seemed to be of importance. Upon treatment of MBF with β-met, there was absence of a protein band at 73 KDa, and subsequently, no nanoparticle formation was observed, suggesting its crucial role in the reduction process. Also, a shorter peptide (25 KDa) was found to be adhered to the

synthesized nanoparticles, suggesting its role in stabilization of nanoparticles. This is in accordance with our recently reported study where we concluded that ionic reduction in some bacteria takes place due to certain proteins along the lipopolysaccharides/cell wall which reduces the metallic ions in its vicinity of the bacterial cell, thereby producing stable nanoparticles [25].

Subsequently, resulting nanoparticles were analysed by TEM and XRD. TEM images (Figure 4a) confirmed the presence of discrete nanoparticles in the range of approximately 50 nm. Some small nanoparticles were also visualized suggesting inherent polydispersity as generally observed in the case of biogenic synthesis. Nanoparticle size was calculated without the encasing membrane-bound proteins. It was observed that the nanoparticles obtained were highly discrete, were circular in shape and did not show aggregation with the neighbouring particles. Also, single-crystalline structures of biogenic nanoparticles were further supported by their corresponding SAED analysis as shown in Figure 4b with characteristic {111}, {200} and {220} diffraction patterns suggesting a face-centred cube (fcc) arrangement.

Finally, confirmation of gold nanoparticles was done via XRD which confirmed the presence of synthesized gold (Figure 5). Bragg's reflections observed in the diffraction pattern could be indexed on the basis of fcc-type crystal arrangement. The strong diffraction peak at 38.21° is ascribed to the {111} facet of the fcc-metal gold structure. The other two peaks can be attributed to {200} and {220} facets at 44.19° and 64.45°, respectively. It is important to note that the ratio of intensity between {200} and {111} peaks is lower than the standard value (0.47 versus 0.53). Also, the ratio between {220} and {111} peaks is lower than the standard value (0.32 versus 0.33). These observations indicate that gold nanoplates (and not nanospheres, although both will exhibit circular plane) were formed in majority by the reduction of Au(III) by membrane-bound fraction of *E. coli* K12 and are dominated by {111} facets. Further, most of the {111} planes parallel to the surface of the supporting substrate were sampled.

Catalytic activity of Au-MBF biocatalyst in 4-nitrophenol degradation

Aqueous 4-NP shows maximum UV–vis absorbance at 317 nm [26]. When NaBH4 (pH > 12) was added to reduce 4-NP, an intense yellow colour appeared due to formation of 4-nitrophenolate ion red-shifting the absorption peak to 400 nm [27]. The reaction does not proceed, and the peak remained for several days in the absence of Au catalyst [28,29]. Also, no peak change was observed in the control reaction consisting of MBF only without Au NPs.

Normally, $-NO_2$-containing aromatic compounds are inert to the reduction via $NaBH_4$. However, with the addition of MBF-Au NP biocatalyst, the colour faded to a colourless solution (as shown in Figure 6a) and the peak at 400 nm decreases with the appearance of the peak at 290 nm corresponding to the formation of 4-AP [30]. Au NPs present in the biocomposite helped in the transfer of electron from BH_4^- ions to the nitro group of 4-NP and reducing it to 4-AP, which was qualitatively monitored by UV–vis spectroscopy as shown in Figure 6b. Since the concentration of bionanocomposite catalysing the reaction was very low, measurement of the absorption spectra of 4-NP and the reduction product 4-AP was not disturbed by the light scattering due to the catalyst carrier particles in the reaction mixture. As the concentration of $NaBH_4$ used was much higher than that of 4-NP, it is assumed that the concentration of BH_4^- remains constant during the reaction, and in this

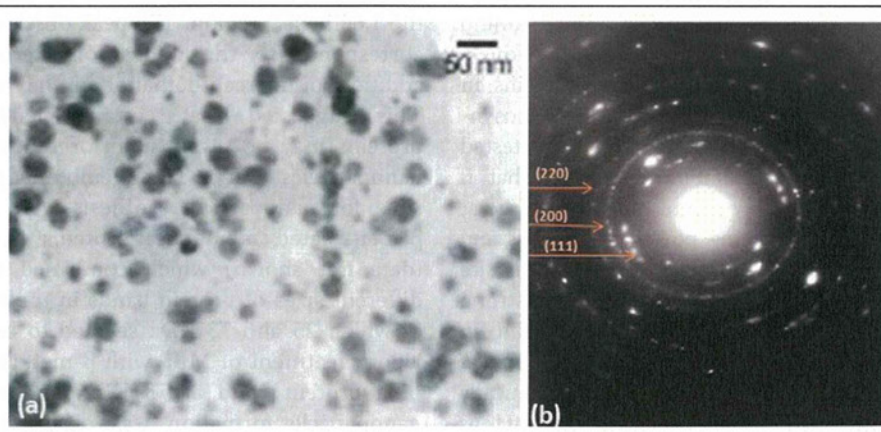

Figure 4 TEM images of biogenic Au nanoparticles after 24 h. (**a**) Discrete gold nanoparticles of size approximately 50 nm; (**b**) SAED pattern of obtained Au NPs.

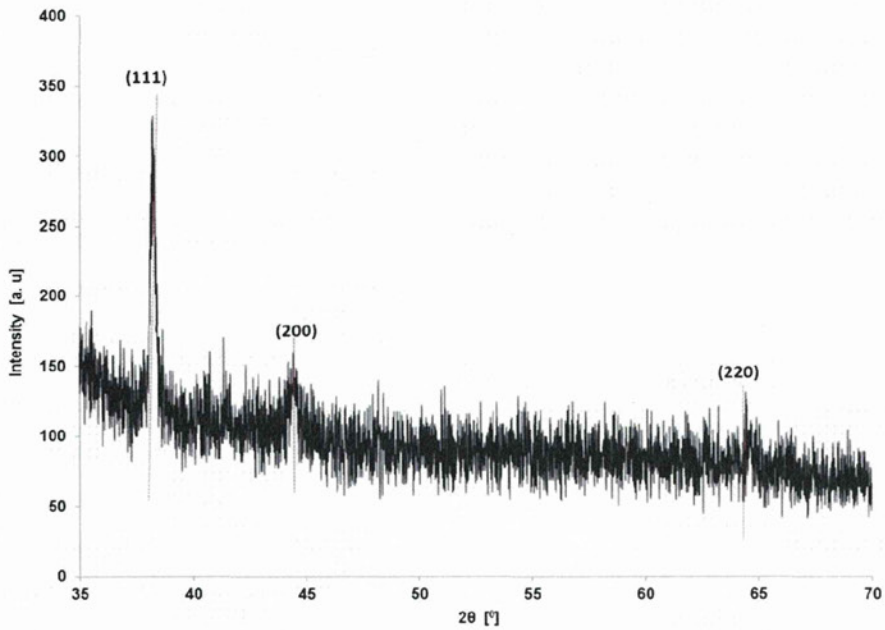

Figure 5 XRD spectra of Au^0 as obtained by membrane-bound fraction of *E. coli* K12 cells.

context, the order of reaction can be considered as a pseudo-first-order reaction [31]. We found good linear correlation of ln(A) and time, and the kinetic reaction rate constant under the given set of reaction conditions was estimated to be 1.24×10^{-2} min^{-1}. However, it should be noted that the reduction rate of 4-NP can be influenced by the concentration of catalyst, size of catalyst, concentration of reactants and temperature [32]. Here, we observed that the biomass-supported catalyst proved to be a sturdy substitute for catalyst matrix as biogenic nanoparticles tend to adhere/adsorb to the biomaterial matrix because of certain active chemical groups, which in turn may impart additional stability to the biocatalyst framework. Further, the biomass alone in the absence of Au NPs was inert to the reaction. This 'green catalyst' will greatly reduce the cost incurred in bioremediation with an added advantage of being a totally eco-friendly synthesis process. Although there may be a few drawbacks like polydispersity of nanoparticles which may affect the quality of nanobiocatalyst, nonetheless considering the economic viability and facile green synthesis, this study helps in better understanding of bacteria-mediated nanoparticle synthesis and associated development of biocatalysts for the reduction of nitroaromatic pollutants.

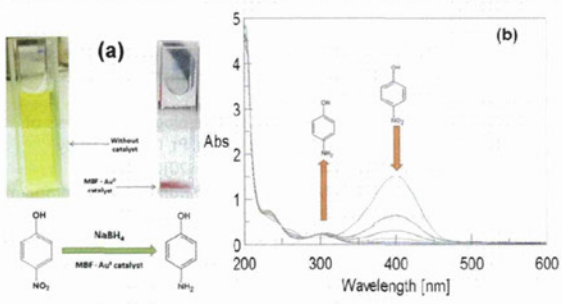

Figure 6 Degradation of 4-nitrophenol and UV–vis absorption spectra. (**a**) Schematic representation of degradation of 4-nitrophenol from pale yellow into colourless solution in the presence of MBF-Au^0 heterogeneous catalyst; (**b**) UV–vis absorption spectra during the reduction of 4-nitrophenolate ion by Au NPs bound to MBF over a time period of 10 min.

Conclusions

Extracellular membrane fraction of *E. coli* K12 was found to be responsible for the biogenic synthesis of gold nanoparticles at room temperature without pH adjustment. Gold nanoplates were obtained in majority in the size range of around 50 nm. We concluded that certain proteins embedded in the membrane fraction cause formation and stabilization of Au NPs. In the absence of these proteins (activity loss by β-met treatment), no nanoparticle formation was observed. Since biogenic nanoparticles are stabilized 'naturally' in the presence of active biomass, their efficacy in the preparation of heterogeneous catalyst was examined. We provided an innovative approach to utilize biogenic gold nanoparticles adsorbed over the cell membrane fraction to be used as a heterogeneous catalyst for catalysing complete degradation of 4-NP. A distinct advantage of this study lies in the fact

that the facile green synthesis process can be seamlessly aligned with the preparation of nanobiocatalyst which may find numerous applications in catalysis, bioremediation studies, etc. This research has the potential to promote membrane fractions (proteins) for continuous synthesis of different types of NPs (see Additional file 1) and subsequent development of associated bionanocomposite resulting in improved material synthesis and application by biogenic systems.

Additional file

Additional file 1: Supplementary information. It contains information about SDS-PAGE and preparation of membrane-bound fraction (MBF) column reactor for continuous synthesis of Au NPs.

Abbreviations

4-AP: 4-aminophenol; 4-NP: 4-nitrophenol; β-met: β-mercaptoethanol; MBF: membrane-bound fraction; NP: nanoparticle.

Competing interests

The authors declare that they have no competing interests.

Authors' contributions

SKS designed the protocol, carried out the experimental analysis and drafted the manuscript. CO and RY provided necessary technical discussions along with manuscript development. AK supervised the research and provided necessary infrastructural support. All authors have read and approved the final manuscript.

Acknowledgements

This work was partly supported by the Special Coordination Fund for Promoting Science and Technology, Creation of Innovative Centers for Advanced Interdisciplinary Research Areas (Innovative BioProduction Kobe) from the Ministry of Education, Culture, Sports and Technology (MEXT) and by the MEXT Scholarship research fund. We also extend our sincere gratitude to Dr. Yasukiyo Ueda for his assistance with TEM observations, Dr. Atsunori Mori for his assistance with FT-IR and Dr. Yuzuru Mizuhata for his assistance with XRD. SKS would like to thank Ms. Charu Srivastava (TCS, India) for her constant support and insightful discussions leading to the completion of this research.

Author details

[1]Department of Chemical Science and Engineering, Graduate School of Engineering, Kobe University, 1-1 Rokkodai-cho, Nada, Kobe 657-8501, Japan. [2]Organization of Advanced Science and Technology, Kobe University, 1-1 Rokkodai-cho, Nada, Kobe 657-8501, Japan.

Received: 28 November 2012 Accepted: 28 January 2013
Published: 12 February 2013

References

1. Bond GC, Thompson DT: **Catalysis by gold.** *Catal Rev Sci Eng* 1995, **41**:319–388.
2. Narayanan R, El-Sayed MA: **Catalysis with transition metal nanoparticles in colloidal solution: nanoparticle shape dependence and stability.** *J Phys Chem B* 2005, **109**:12663–12676.
3. Daniel MC, Astruc D: **Gold nanoparticles: assembly, supramolecular chemistry, quantum-size-related properties and applications toward biology, catalysis, and nanotechnology.** *Chem Rev* 2004, **104**:293–346.
4. Murphy CJ, Sau TK, Gole AM, Orendorff CJG, Gou JL, Hunyadi SE, Li T: **Anisotropic metal nanoparticles: synthesis, assembly, and optical applications.** *J Phys Chem B* 2005, **109**:13857–13870.
5. Pileni MP: **The role of soft colloidal templates in controlling the size and shape of inorganic nanocrystals.** *Nat Mater* 2003, **2**:145–149.
6. Brust M, Kiely CJ: **Some recent advances in nanostructure preparation from gold and silver particles: a short topical review.** *Colloid Surface A* 2002, **202**:175–186.
7. Genc R, Clergeaud G, Ortiz M, O'Sullivan CK: **Green synthesis of gold nanoparticles using glycerol-incorporated nanosized liposomes.** *Langmuir* 2011, **27**:10894–10900.
8. Ogi T, Saitoh N, Nomura T, Konishi Y: **Room-temperature synthesis of gold nanoparticles and nanoplates using *Shewanella algae* cell extract.** *J Nanopart Res* 2010, **12**:2531–2539.
9. Nair B, Pradeep T: **Coalescence of nanoclusters and formation of submicron crystallites assisted by *Lactobacillus* strains.** *Cryst Growth Des* 2002, **2**:293–298.
10. Gericke M, Pinches A: **Microbial production of gold nanoparticles.** *Gold Bull* 2006, **39**:22–28.
11. Das SK, Das AR, Guha AK: **Gold nanoparticles: microbial synthesis and application in water hygiene management.** *Langmuir* 2009, **25**:8192–8199.
12. Thakkar KN, Mhatre SS, Parikh RY: **Biological synthesis of metallic nanoparticles.** *Nanomed-Nanotechnol* 2010, **6**:257–262.
13. Narayanan KB, Sakthivel N: **Biological synthesis of metal nanoparticles by microbes.** *Adv Colloid Interface Sci* 2010, **156**:1–13.
14. Booth G: *Nitro Compounds, Aromatic in Ullmann's Encyclopedia of Industrial Chemistry.* New York: Wiley; 2007.
15. Pohanish RP: *Sittig's Handbook of Toxic and Hazardous Chemicals and Carcinogens.* Amsterdam: Elsevier; 2011.
16. Haruta M: **Size and support dependency in the catalysis of gold.** *ChemInform* 1997, **28**:153–166.
17. Deplanche K, Merroun ML, Casadesus M, Tran DT, Mikheenko IP, Bennett JA, Zhu J, Jones IP, Attard GA, Wood J, Selenska-Pobell S, Macaskie LE: **Microbial synthesis of core/shell gold/palladium nanoparticles for applications in green chemistry.** *J R Soc Interface* 2012, **9**:1705–1712.
18. Pazirandeh M, Wells BM, Ryan RL: **Development of bacterium-based heavy metal biosorbents: enhanced uptake of cadmium and mercury by *Escherichia coli* expressing a metal binding motif.** *Appl Environ Microbiol* 1998, **64**:4068–4072.
19. Ackerley DF, Barak Y, Lynch SV, Curtin J, Matin A: **Effect of chromate stress on *Escherichia coli* K-12.** *J Bacteriol* 2006, **188**:3371–3381.
20. Narayanan KB, Sakthivel N: **Synthesis and characterization of nano-gold composite using *Cylindrocladium floridanum* and its heterogeneous catalysis in the degradation of 4-nitrophenol.** *J Hazard Mater* 2011, **189**:519–525.
21. Link S, El-Sayed MA: **Shape and size dependence of radiative, nonradiative, and photothermal properties of gold nanocrystals.** *Int Rev Phys Chem* 2000, **19**:409–453.
22. Basu S, Panigrahi S, Praharaj S, Ghosh SK, Pande S, Jana S, Pal T: **Dipole–dipole plasmon interactions in self-assembly of gold organosol induced by glutathione.** *New J Chem* 2006, **30**:1333–1339.
23. Gole A, Dash C, Ramachandran V, Mandale AB, Sainkar SR, Mandale AB, Rao M, Sastry M: **Pepsin–gold colloid conjugates: preparation, characterization and enzymatic activity.** *Langmuir* 2001, **17**:1674–1679.
24. He S, Guo Z, Zhang Y, Zhang S, Wang J, Gu N: **Biosynthesis of gold nanoparticles using the bacteria *Rhodopseudomonas* capsulate.** *Mater Lett* 2007, **61**:3984–3987.
25. Srivastava SK, Constanti M: **Room temperature biogenic synthesis of multiple nanoparticles (Ag, Pd, Fe, Rh, Ni, Ru, Pt, Co, and Li) by *Pseudomonas aeruginosa* SM1.** *J Nanopart Res* 2012, **14**:831.
26. Pradhan N, Pal A, Pal T: **Catalytic reduction of aromatic nitro compounds by coinage metal nanoparticles.** *Langmuir* 2001, **17**:1800–1802.
27. Ghosh SK, Mandal M, Kundu S, Nath S, Pal T: **Bimetallic Pt-Ni nanoparticles can catalyze reduction of aromatic nitro compounds by sodium borohydride in aqueous solution.** *Appl Catala-Gen* 2004, **268**:61–66.
28. Hayakawa K, Yoshimura T, Esumi K: **Preparation of gold–dendrimer nanocomposites by laser irradiation and their catalytic reduction of 4-nitrophenol.** *Langmuir* 2003, **19**:5517–5521.
29. Lu Y, Mei Y, Ballauff M: **Thermosensitive core–shell particles as carrier systems for metallic nanoparticles.** *J Phys Chem B* 2006, **110**:3930–3937.
30. Pradhan N, Palb A, Pal T: **Silver nanoparticle catalyzed reduction of aromatic nitro compounds.** *Colloid Surface A* 2002, **196**:247–257.

31. Scott RWJ, Wilson OM, Crooks RM: **Synthesis, characterization and applications of dendrimer-encapsulated nanoparticles.** *J Phys Chem B* 2005, **109**:692–704.
32. Panigrahi S, Basu S, Praharaj S, Pande S, Jana S, Pal A, Ghosh SK, Pal T: **Synthesis and size-selective catalysis by supported gold nanoparticles: study on heterogeneous and homogeneous catalytic process.** *J Phys Chem C* 2007, **111**:4596–460.

doi:10.1186/1556-276X-8-70
Cite this article as: Srivastava *et al.*: Biogenic synthesis and characterization of gold nanoparticles by *Escherichia coli* K12 and its heterogeneous catalysis in degradation of 4-nitrophenol. *Nanoscale Research Letters* 2013 **8**:70.

(This is a sample cover image for this issue. The actual cover is not yet available at this time.)

Materials Letters 79 (2012) 78–80

Contents lists available at SciVerse ScienceDirect

Materials Letters

journal homepage: www.elsevier.com/locate/matlet

Directed assembly of metal oxide nanoparticles by DNA

Jinghua Han [a,b], Satoshi Ohara [a,*], Kazuyoshi Sato [c], Hui Xu [d], Zhenquan Tan [a], Yoshiaki Morisada [a], Kazuo Kuruma [a], Makio Naito [a], Ping Shan [b], Mitsuo Umetsu [e]

[a] Joining and Welding Research Institute, Osaka University, 11-1 Mihogaoka, Ibaraki, Osaka 567-0047, Japan
[b] School of Material Science and Engineering, Tianjin University, No.92, Weijin Road, Nankai District, Tianjin City 300072, China
[c] Department of Chemical & Environmental Engineering, Graduate School of Engineering, Gunma University, 1-5-1 Tenjin-cho, Kiryu, Gunma 376-8515, Japan
[d] School of Pharmacy, Shenyang Pharmaceutical University, No.103, Wenhua Road, Shenhe District, Shenyang City, Liaoning Province, China
[e] Department of Biomolecular Engineering, Graduate School of Engineering, Tohoku University, 6-6-11 Aoba, Aramaki, Aoba-ku, Sendai, Miyagi 980-8579, Japan

ARTICLE INFO

Article history:
Received 28 December 2011
Accepted 24 March 2012
Available online 31 March 2012

Keywords:
Assembly
Zirconia
Nanoparticles
DNA

ABSTRACT

Directed assembly of metal oxide nanoparticles with the aid of DNA was investigated. One-dimensional arrangement of zirconia (ZrO_2) nanoparticles using DNA as a template was shown by TEM observation. It is considered that the DNA-directed assembly of ZrO_2 nanoparticles is due to the Coulomb interactions between the negatively charged DNA and positively charged ZrO_2 nanoparticles.

1. Introduction

When used as building blocks for nanostructures, nanoparticles make further miniaturization of structures and devices possible [1]. Recently assembling nanoparticles on the nanoscale has received considerable attention [2–11], and one tool for creating these assemblies is biomaterials. Deoxyribonucleic acid (DNA) is an appropriate biopolymer template for constructing defined inorganic materials, and highly selective base-pairing interactions between complementary single-strand DNA chains have been used in nanoassemblies. Additionally, native double-helical DNA can directly interact with metal ions and their complexes, and the role of DNA in assembling metal nanoparticles has been reported [12–20]. Recently, assembly of metal oxide nanoparticles has been demonstrated by surfactant capping on the nanoparticles [21,22]. However, DNA-directed assembly of metal oxide nanoparticles remains a challenge.

Metal oxide ceramic nanoparticles have been extensively investigated due to their successful applications and potential in various fields such as electronics, catalysis, pharmaceutics, energy storage, and medical applications, and using DNA to assemble metal oxide nanoparticles may allow novel hybrid nano-biomaterials with synergetic properties and functions to be realized. Zirconia (ZrO_2) is an attractive ceramic material due to its excellent mechanical, tribological and thermal properties, and good oxygen ionic conductivity. Its nanoparticles have a broad range of applications, including thermal barrier coatings, solid-state electrolytes, solid oxide fuel cells, oxygen sensors, and heterogeneous catalysts etc. [23–29]. From the viewpoint of several key applications, the assembly of ZrO_2 ceramic nanoparticles has been eagerly anticipated. The aim of this communication is to elucidate the directed assembly of ZrO_2 nanoparticles with the aid of DNA. Herein, we show the first example of a one-dimensional arrangement of metal oxide nanoparticles without surfactant capping using DNA as a template.

2. Experimental

The ZrO_2 ceramic nanoparticles, which were synthesized by a hydrothermal reaction, were a colloidal solution. Aqueous solution of $ZrOCl_2 \cdot 8H_2O$ was mixed with $KHCO_3$/KOH solution. Then the solution was hydrothermally treated at 150 °C for 1 h in the Teflon lined stainless steel vessel. The detailed hydrothermal synthesis is described in a previously reported method [30]. After the reaction, ZrO_2 nanoparticles in the solution were purified by washing ten times with deionized water and 5 M of HCl was added to the product for dispersion of the nanoparticles in water. The particle size distribution of the obtained ZrO_2 nanoparticle colloidal solution was measured by the dynamic light scattering (DLS) method, whereas transmission electron microscopy (TEM) was used to observe the ZrO_2 nanoparticles and their assembled nanostructures.

Two types of DNA solutions were used in this study: λ-DNA and a short DNA fragment. The ZrO_2 nanoparticles were assembled by λ-DNA as follows. λ-DNA, which was 48,502 base-pairs (bp) long, was purchased from TaKaRa Biotechnology (Dalian) Co., Ltd. The original concentration

* Corresponding author. Tel./fax: +81 6 6879 4370.
E-mail address: ohara@jwri.osaka-u.ac.jp (S. Ohara).

0167-577X/$ – see front matter © 2012 Elsevier B.V. All rights reserved.
doi:10.1016/j.matlet.2012.03.094

was 0.3 μg/μL, and the equivalent base pair concentration was 450 μmol/L. The buffer was 10 mmol Tris–HCl–1 mmol EDTA, pH = 8.0, A260/A280 = 1.8–2.0 (DNA purity). A260 and A280 are the optical spectrometer measurement of absorbance at the wavelengths of 260 nm and 280 nm, respectively. The λ-DNA solution (450 μmol/L bp concentration) was diluted to a 1 μmol/L bp concentration by adding a 0.0025 mol/L HCl solution to maintain the pH of λ-DNA near 3.0. A 900 μL ZrO_2 solution (concentration 50 μmol/L) with a HCl solution was prepared to maintain a constant pH value of 3.0. Then 900 μL ZrO_2 solution was added to the 900 μL solution of 0.5 μmol/L bp λ-DNA to make a 1800 μL compound solution of 0.25 μmol/L bp λ-DNA.

The short DNA fragment, which was 50 bp linear and double-stranded, was purchased from Lonza Rockland Inc. To realize a pH of 3.0, the 100 μL short DNA fragment of 138.5 μmol/L was diluted ten-fold to a 1000 μL solution of 13.85 μmol/L with HCl solution (0.0025 mol/L). In the same manner, the zirconia solution (11.3 mmol/L) was diluted two thousand times with a HCl solution to make a 1000 μL solution with a zirconia concentration of 5.65 μmol/L. Then 1000 μL zirconia solution was added to the 1000 μL short DNA fragment solution to yield a mixed solution with a pH of 2.8. The absorption spectrum and zeta potential of DNA solutions were evaluated using an ultraviolet–visible (UV–vis) scanning spectrometer and a zeta potential analyzer, respectively.

3. Results and discussion

Fig. 1a and b shows a photograph and particle size distribution of the obtained transparent ZrO_2 colloidal solution. The ZrO_2 nanoparticle surface contains numerous positive charges at a pH value of 3 because the isoelectric point of ZrO_2 ceramic is around 5–6, and due to the electric repulsion force in water, each ZrO_2 nanoparticle is assumed to be dispersed separately. The average diameter of the ZrO_2 nanoparticle is about 5 nm, and has a very narrow particle distribution (Fig. 1b). Fig. 1c shows a TEM picture of the ZrO_2 nanoparticles. Although the primary ZrO_2 nanoparticles on the TEM grid aggregate after drying the colloidal solution, the primary nanoparticles are about 5 nm, which is consistent with that measured by DLS. Hence, it is concluded that the ZrO_2 nanoparticles can be dispersed perfectly in water under this low pH condition.

Fig. 2 shows the TEM picture of the mixed solution of ZrO_2 nanoparticles and λ-DNA, and indicates that a network is formed as the ZrO_2 nanoparticles are assembled on the DNA strands. In contrast, without DNA, the ZrO_2 nanoparticles are aggregated randomly on the TEM grid (Fig. 1c). However, the ZrO_2 nanoparticles are arranged in the presence of λ-DNA and the morphology agrees well with the assembly of metal nanoparticles by λ-DNA [13,20]. This TEM observation suggests that DNA plays an active role in the directed assembly process of ZrO_2 nanoparticles.

The length of the λ-DNA molecule is very long compared to the size of ZrO_2 ceramic nanoparticles. Thus, to confirm that the ZrO_2 nanoparticles are arranged on DNA, a short DNA fragment with a short length was used. 50 bp of the short DNA fragment corresponds to 17 nm, because the length of one bp is 0.34 nm. Fig. 3 shows the TEM picture of ZrO_2 nanoparticles assembled on the short DNA fragment, and illustrates that several ZrO_2 nanoparticles form an array on the short DNA. Although some ZrO_2 arrays aggregate each other, the ZrO_2 nanoparticles are aligned along the DNA template, as seen in Fig. 3, which reflects the linear morphology of the DNA.

The absorption spectrum and zeta potential of DNA in the working buffer were measured in order to consider the interaction between the DNA molecules and the ZrO_2 nanoparticles. It is thought that the short DNA fragment is stable in the acidic solution, because the absorption property around at 270 nm is not changed in comparison with that in the water. Then, it is confirmed that the short DNA fragment has negative charge even in the acidic solution. Futhermore, when the concentartion of the short DNA fragment increases, each ZrO_2 nanoparticle is individually observed on the TEM grid (Fig. 4). Therefore, the one-

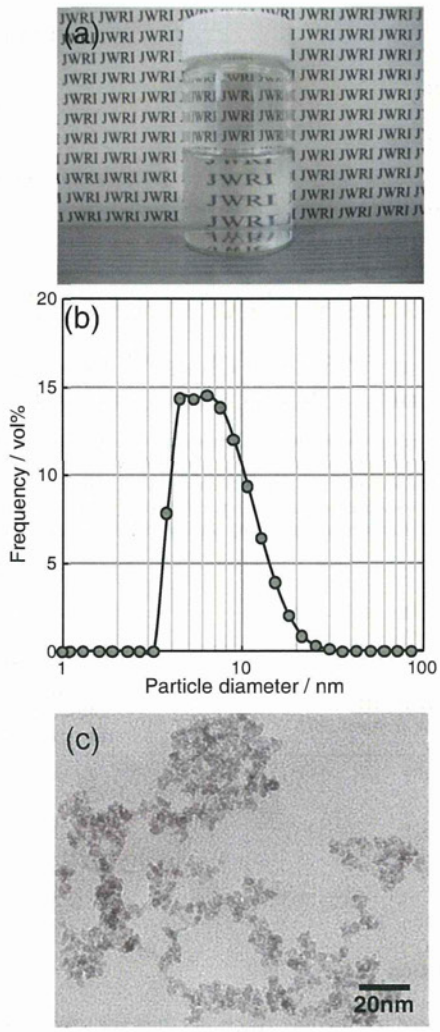

Fig. 1. (a) Photograph and (b) particle size distribution of the synthesized transparent zirconia nanoparticles in water. (c) TEM image of the synthesized zirconia nanoparticles.

dimensional (1D) arrangement is likely due to the Coulomb interactions between the negatively charged DNA and positively charged ZrO_2 nanoparticles.

To date, some groups have reported the assembly of metal oxide nanoparticles by DNA templates [21,22]. However, both nanoparticles were capped by surfactant such as tetramethylammonium hydroxide

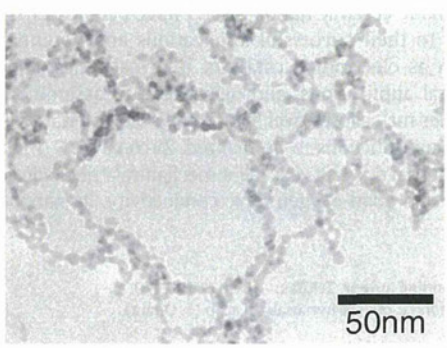

Fig. 2. TEM image of a zirconia nanoparticle assembly by λ-DNA.

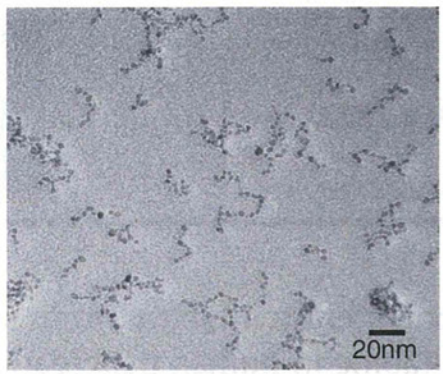

Fig. 3. TEM image of the zirconia nanoparticle assembly by a short DNA fragment. Concentration of the DNA is 13.85 μmol/L.

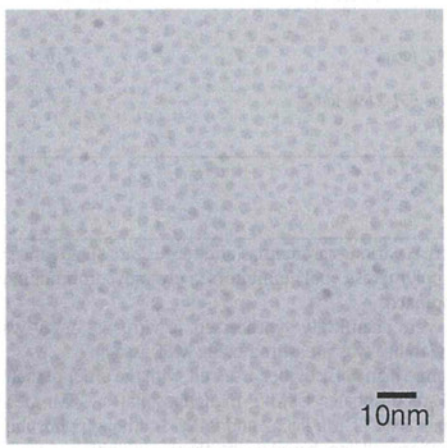

Fig. 4. TEM image of the zirconia nanoparticle assembly by a short DNA fragment. Concentration of the DNA is 138.5 μmol/L.

(TMAH) or cetyltrimethylammonium bromide (CTAB) in order to improve their dispersibility in solution, and the surfactant played an important role in assembling the nanoparticles on DNA. In contrast, the ZrO_2 nanoparticles used in this study are very stable in water without surfactant capping. Hence, we succeeded in DNA-directed assembly of metal oxide nanoparticles for the first time.

4. Conclusion

The role of DNA in assembling metal oxide nanoparticles without surfactant capping was investigated. ZrO_2 nanoparticles are assembled on DNA by Coulomb interactions between the negatively charged DNA and positively charged ZrO_2 nanoparticles. We believe that this directed assembly of metal oxide nanoparticles by DNA will yield novel hybrid nano-biomaterials with synergetic properties and functions.

Acknowledgment

This research was partly supported by a Scientific Research Grant and Grant-in-Aid for Cooperative Research Project of Advanced Materials Development and Integration of Novel Structured Metallic and Inorganic Materials from the Ministry of Education, Culture, Sports, Science and Technology of Japan.

References

[1] Schmid G, editor. Nanoparticles. Wiley-VCH Weinheim; 2004.
[2] Bae AH, Numata M, Hasegawa T, Li C, Kaneko K, Sakurai K, et al. Angew Chem Int Ed 2005;44:2030–3.
[3] Fu AH, Micheel CM, Cha J, Chang H, Yang H, Allivisatos AP. J Am Chem Soc 2004;126:10832–3.
[4] Nakao H, Shiigi H, Yamamoto Y, Tokonami S, Nagaoka T, Sugiyama S, et al. Nano Lett 2003;3:1391–4.
[5] Mirkin CA, Letsinger RL, Mucie RC, Storhoff JJ. Nature 1996;382:607–9.
[6] Sato K, Hosokawa K, Maeda M. J Am Chem Soc 2003;125:8102–3.
[7] Gu Q, Cheng C, Haynie DT. Nanotechnology 2005;16:1358–63.
[8] Braun E, Eichen Y, Sivan U, Ben-Yoseph G. Nature 1998;392:775–8.
[9] Zinchenko AA, Yoshikawa K, Baigl D. Adv Mater 2005;17:2820–3.
[10] Kumar A, Pattarkine M, Bhadbhade M, Mandale AB, Ganesh KN, Datar SS, et al. Adv Mater 2001;13:341–4.
[11] Xiao SJ, Liu FR, Rosen AE, Hainfeld JF, Seeman NC, Musier-Forsyth K, et al. J Nanopart Res 2002;4:313–7.
[12] Richter J, Merig M, Pompe W, Monch I, Schackert HK. Appl Phys Lett 2001;78:536–8.
[13] Richter J, Seidel R, Kirsch R, Mertig M, Pompe W, Plaschke J, et al. Adv Mater 2000;12:507–10.
[14] Ford WE, Harnack O, Yasuda A, Wessels JM. Adv Mater 2001;12:1793–7.
[15] Mertig M, Ciacchi LC, Seidel R, Pompe W, De Vita A. Nano Lett 2002;2:841–4.
[16] Keren K, Krueger M, Gilad R, Ben-Yoseph G, Sivan U, Braun E. Science 2002;297:72–5.
[17] Keren K, Berman RS, Braun E. Nano Lett 2004;4:323–6.
[18] Monson CF, Woolley AT. Nano Lett 2003;3:359–63.
[19] Becerril HA, Stoltenberg RM, Monson CF, Woolley AT. J Mater Chem 2004;14:611–6.
[20] Hatakeyama Y, Umetsu M, Ohara S, Kawadai F, Takami S, Naka T, et al. Adv Mater 2008;20:1122–8.
[21] Nyamjav D, Ivanisevic A. Biomaterials 2005;26:2749–57.
[22] Wang L, Wei G, Qi B, Zhou H, Liu Z, Song Y, et al. Appl Surf Sci 2006;252:2711–6.
[23] Ye Z, Tan M, Wang G, Yuan J. J Fluoresc 2005;15:499–505.
[24] Limaye AU, Helble JJ. J Am Ceram Soc 2002;85:1127–32.
[25] Schmidt T, Menning M, Schmidt H. J Am Ceram Soc 2007;90:1401–5.
[26] Trunec M, Maca K. J Am Ceram Soc 2007;90:2735–40.
[27] Shankar SS, Joshi H, Pasricha R, Pavaskar NR, Mandale AB, Sastry M. J Colloid Interface Sci 2004;269:126–30.
[28] Matsui K, Ohgai M. J Am Ceram Soc 2001;84:2303–12.
[29] Hannink RHJ, Kelly PM, Muddle BC. J Am Ceram Soc 2000;83:461–87.
[30] Sato K, Abe H, Ohara S. J Am Chem Soc 2010;13:2538–9.

Biochimica et Biophysica Acta 1830 (2013) 2517–2525

Contents lists available at SciVerse ScienceDirect

Biochimica et Biophysica Acta

journal homepage: www.elsevier.com/locate/bbagen

Monogalactosyl diacylglycerol, a replicative DNA polymerase inhibitor, from spinach enhances the anti-cell proliferation effect of gemcitabine in human pancreatic cancer cells

Hiroaki Akasaka [a], Ryohei Sasaki [a], Kenji Yoshida [a], Izumi Takayama [a], Toyofumi Yamaguchi [b], Hiromi Yoshida [c], Yoshiyuki Mizushina [c,d,*]

[a] Division of Radiation Oncology, Kobe University Graduate School of Medicine, Chuo-ku Kobe, Hyogo 650-0017, Japan
[b] Department of Life & Health Sciences, Teikyo University of Science, Adachi-ku, Tokyo 120-0045, Japan
[c] Laboratory of Food & Nutritional Sciences, Faculty of Nutrition, Kobe Gakuin University, Nishi-ku, Kobe, Hyogo 651-2180, Japan
[d] Cooperative Research Center of Life Sciences, Kobe Gakuin University, Chuo-ku, Kobe, Hyogo 650-8586, Japan

ARTICLE INFO

Article history:
Received 22 June 2012
Received in revised form 25 October 2012
Accepted 10 November 2012
Available online 19 November 2012

Keywords:
Monogalactosyl diacylglycerol (MGDG)
Gemcitabine (GEM)
DNA polymerase (pol)
Enzyme inhibitor
Anticancer
Apoptosis

ABSTRACT

Background: Gemcitabine (GEM) is used to treat various carcinomas and represents an advance in pancreatic cancer treatment. In the screening for DNA polymerase (pol) inhibitors, a glycoglycerolipid, monogalactosyl diacylglycerol (MGDG), was isolated from spinach.
Methods: Phosphorylated GEM derivatives were chemically synthesized. *In vitro* pol assay was performed according to our established methods. Cell viability was measured using MTT assay.
Results: Phosphorylated GEMs inhibition of mammalian pol activities assessed, with the order of their effect ranked as: GEM-5′-triphosphate (GEM-TP) > GEM-5′-diphosphate > GEM-5′-monophosphate > GEM. GEM suppressed growth in the human pancreatic cancer cell lines BxPC-3, MIAPaCa2 and PANC-1 although phosphorylated GEMs showed no effect. MGDG suppressed growth in these cell lines based on its selective inhibition of replicative pol species. Kinetic analysis showed that GEM-TP was a competitive inhibitor of pol α activity with nucleotide substrates, and MGDG was a noncompetitive inhibitor with nucleotide substrates. GEM combined with MGDG treatments revealed synergistic effects on the inhibition of DNA replicative pols α and γ activities compared with GEM or MGDG alone. In cell growth suppression by GEM, pre-addition of MGDG significantly enhanced cell proliferation suppression, and the combination of these compounds was found to induce apoptosis. In contrast, GEM-treated cells followed by MGDG addition did not influence cell growth.
Conclusions: GEM/MGDG enhanced the growth suppression of cells based on the inhibition of pol activities.
General significance: Spinach MGDG has great potential for development as an anticancer food compound and could be an effective clinical anticancer chemotherapy in combination with GEM.

1. Introduction

Cancer is a major, worldwide, public health problem, and epidemiologic and animal studies have indicated that vegetables and fruits with chemopreventive natural products, alone or in mixtures, are associated with reducing the risk of developing cancer [1–3]. DNA polymerase (DNA-dependent DNA polymerase [pol], E.C. 2.7.7.7) catalyzes deoxyribonucleotide addition to the 3′-hydroxyl terminus of primed double-stranded DNA molecules [4]. As pols play important maintenance roles in key eukaryotic systems, such as DNA replication, recombination and repair [5], pol inhibitors can be employed as anticancer chemotherapy agents because they inhibit cell proliferation. Based on pol inhibitors' strategic effects, we have been screening for mammalian pol inhibitors from natural phytochemical products in vegetables and fruits for over 15 years.

The human genome encodes at least 15 DNA pols that conduct cellular DNA synthesis [6,7]. Eukaryotic cells contain 3 replicative pols (α, δ and ε), 1 mitochondrial pol (γ), and at least 11 non-replicative pols (β, ζ, η, θ, ι, κ, λ, μ, ν, terminal deoxynucleotidyl transferase (TdT) and REV1) [8,9]. Pols have a highly conserved structure, with their overall catalytic subunits showing little variance among species; conserved enzyme structures are usually preserved over time because they perform important cellular functions that confer evolutionary advantages. On the

Abbreviations: pol, DNA-dependent DNA polymerase (E.C. 2.7.7.7); MGDG, monogalactosyl diacylglycerol; GEM, gemcitabine; GEM-TP, gemcitabine-5′-triphosphate; GEM-DP, gemcitabine-5′-diphosphate; GEM-MP, gemcitabine-5′-monophosphate; dTTP, 2′-deoxythymidine-5′-triphosphate; dNTP, 2′-deoxynucleotide-5′-triphosphate; DMSO, dimethyl sulfoxide; PBS, phosphate-buffered saline; FBS, fetal bovine serum; ssDNA, single-stranded DNA; IC_{50}, 50% inhibitory concentration; LD_{50}, 50% lethal dose

* Corresponding author at: Laboratory of Food & Nutritional Sciences, Faculty of Nutrition, Kobe Gakuin University, Nishi-ku, Kobe, Hyogo 651-2180, Japan. Tel.: +81 78 974 1551x3232; fax: +81 78 974 5689.
E-mail address: mizushin@nutr.kobegakuin.ac.jp (Y. Mizushina).

0304-4165/$ – see front matter © 2012 Elsevier B.V. All rights reserved.
http://dx.doi.org/10.1016/j.bbagen.2012.11.004